High-energy cosmic ray production in X-ray binary jets

Cooper, A.J.; Gaggero, D.; Markoff, S.; Zhang, S.

DOI
10.1093/mnras/staa373

Publication date
2020

Document Version
Final published version

Published in
Monthly Notices of the Royal Astronomical Society

Monthly Notices of the ROYAL ASTRONOMICAL SOCIETY

MNRAS **493,** 3212–3222 (2020) doi:10.1093/mnras/staa373
Advance Access publication 2020 February 11

High-energy cosmic ray production in X-ray binary jets

A. J. Cooper [1,2,3★] D. Gaggero,[1,4] S. Markoff[1,2] and S. Zhang[5,6]

[1]*GRAPPA, Gravitational and Astroparticle Physics Amsterdam, University of Amsterdam, Science Park 904, NL-1098 XH Amsterdam, the Netherlands*
[2]*Anton Pannekoek Institute for Astronomy (API), University of Amsterdam, Science Park 904, NL-1098 XH Amsterdam, the Netherlands*
[3]*ASTRON, Netherlands Institute for Radio Astronomy, Oude Hoogeveensedijk 4, NL-7991 PD Dwingeloo, the Netherlands*
[4]*Instituto de Física Teórica UAM/CSIC, Calle Nicolás Cabrera 13–15, Cantoblanco, E-28049 Madrid, Spain*
[5]*Institute for Astrophysical Research, Boston University, 725 Commonwealth Avenue, Boston, MA 02215, USA*
[6]*Physics Program, Bard College, 30 Campus Road, Annandale-on-Hudson, NY 12504, USA*

Accepted 2020 February 2. Received 2020 January 30; in original form 2019 October 18

ABSTRACT

As smaller analogues of active galactic nuclei, X-ray binaries (XRBs) are also capable of launching jets that accelerate particles to high energies. In this work, we re-examine XRB jets as potential sources of high-energy cosmic rays (CRs) and explore whether they could provide a significant second Galactic component to the CR spectrum. In the most intriguing scenario, XRB-CRs could dominate the observed spectrum above the so-called knee feature at $\sim 3 \times 10^{15}$ eV, offering an explanation for several key issues in this transition zone from Galactic to extragalactic CRs. We discuss how such a scenario could be probed in the near future via multimessenger observations of XRB jets, as well as diffuse Galactic neutrino flux measurements.

Key words: acceleration of particles – astroparticle physics – cosmic rays – ISM: jets and outflows – Galaxy: centre.

1 INTRODUCTION

The origin of cosmic rays (CRs), high-energy particles from beyond the Solar system, is a century-old puzzle (Ginzburg & Syrovatskii 1964; Berezinsky et al. 1990; Blasi 2013). We are yet to firmly identify classes of astrophysical sources able to accelerate hadronic cosmic particles up to extremely high energies, much larger than those accessible by terrestrial accelerators.

Spectral features in the locally observed all-particle CR spectrum can shed light on this mystery. The observed spectrum follows a power law with an index of $p \approx -2.7$ over many decades of energy. However, over years of observation, small deviations with respect to the power law have been identified as follows: the *knee*, a softening of the spectra at 3×10^{15} eV; the *second knee*, a further softening at around 2×10^{17} eV; and the *ankle*, a hardening of the spectrum occurring at roughly 4×10^{18} eV (Blasi 2013).

It is commonly thought that Galactic sources are able to accelerate hadrons up to the knee, with supernova remnant (SNR) shocks as the prime candidates, yet many aspects of this picture are far from clear. CR paths are deflected in the Galactic magnetic field and therefore we cannot directly trace them back to their source. To this end, indirect 'smoking gun' signals, including characteristic TeV γ-ray spectra from pion decay channels, can be observed to verify CR acceleration sites. Although observations of X-ray filaments (Vink & Laming 2003) and γ-ray spectra from old SNRs (Ackermann et al. 2013) suggest that protons are efficiently accelerated at these sources, it is not clear whether SNRs can universally attain the crucial PeV energies required to explain the softening at the knee (see e.g. the recent discussion in Gabici, Gaggero & Zandanel 2016; Ahnen et al. 2017b, and references therein). In the context of the SNR hypothesis, one of the key ideas to explain the knee and second knee features is rigidity-dependent diffusive shock acceleration, in which the maximum possible energy of a given CR species depends on its atomic number Z such that $E_{\rm max}(Z) = Z \times E_{\rm max}(1)$. This has had success in explaining the second knee feature in terms of the cut-off of accelerated iron nuclei, as extensively discussed in the literature for many decades (see e.g. the early discussion in Peters 1961).

Besides the nature of the knee, we are still left with many open issues regarding the potential Galactic CR component. In particular, the origin of CRs between second knee and ankle, and the location of the transition from Galactic to extragalactic CRs remain unclear. One possibility is that the extragalactic component is dominant all the way down to 10^{17} eV, requiring the ankle feature to be a peculiar extragalactic propagation effect. However, alternative models also exist, mostly based on the assumption of energy-dependent leakage of high-energy CRs from the Galaxy (see for instance, Giacinti, Kachelrieß & Semikoz 2015), which look to negate the need for an extragalactic CR component to dominate down to the second knee. Another option that has been put forward is the existence of a second Galactic component that 'fills the gap' (see Fig. 1). Taking this additional component into account, as discussed in Hillas (2005) and Gaisser, Stanev & Tilav (2013), it is possible to provide a complete and consistent description of all the features from the knee to the ankle. Possible candidates for such high-energy Galactic components include strong Galactic winds (Jokipii & Morfill 1987), newborn pulsars (Fang, Kotera & Olinto 2013), Galactic γ-ray bursts (Levinson & Eichler 1993), Wolf–Rayet star supernovae (SNe; Thoudam et al. 2016), and many others.

Recently, this idea of a second Galactic CR component has been bolstered by new composition measurements that favour a strong light composition at around 10^{17} eV. For instance, in Buitink et al.

★ E-mail: a.j.cooper@uva.nl

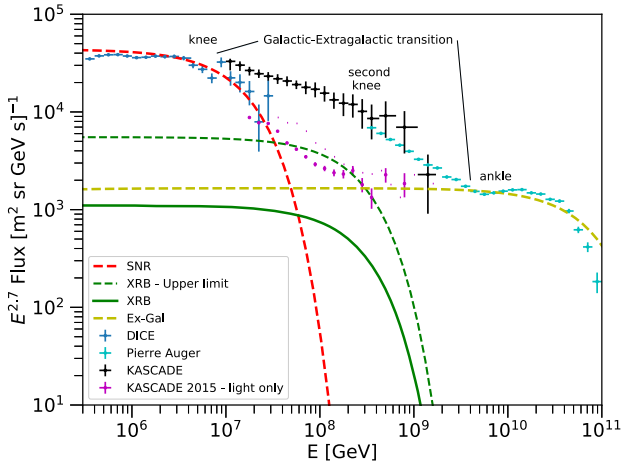

Figure 1. Schematic of a three-component all-particle CR spectrum. The components are SNR-CRs (red), X-ray binary (XRB)-CRs (this work; green), and a canonical extragalactic component (yellow). The green line reflects an XRB-CR contribution with a total power of approximately 10^{38} erg s^{-1}, using the reasonable parameters in the middle column of Table 1. The dashed green line represents the upper limit of the allowed XRB-CR power as discussed in Section 3, using the upper parameters in Table 1. Such a contribution is dominant around 10^{16}–10^{17} eV, and could be probed via composition measurements. Here, we have assumed that all sources share the same power-law index of accelerated CRs. Allowing slightly harder spectra for XRB-CRs means they could explain the entire CR flux at the second knee without violating energetic constraints.

(2016), a novel data set based on 150 d of radio observations of CR-induced extensive air showers made with the Low-Frequency Array implies a significant light-mass component in the $10^{17}-10^{17.5}$ eV range. The authors suggest this composition dip likely necessitates a primarily proton-dominated Galactic component that can reach approximately these energies. Measurements from different types of surface detectors, including HiRes, Auger, Telescope Array, and KASCADE-Grande data (Pierre Auger Collaboration 2014; Hanlon 2019; reviewed in e.g. Kampert & Unger 2012), are compatible with these recent findings, and clearly outline a decrease of the average mass of CRs towards the ankle.

In this paper, we follow this line of inquiry and explore whether XRB jets, given the expected total overall power and maximum energy cut-off, could be viable candidates for the second Galactic source of CRs. CR acceleration in XRB jets has been previously explored by Heinz & Sunyaev (2002) and later by Fender, Maccarone & van Kesteren (2005), yet largely neglected since. In light of increasingly detailed multiwavelength studies of many more XRB jets (Corral-Santana et al. 2016; Tetarenko et al. 2016a), which help constrain population statistics, as well as in anticipation of the next generation of very high-energy (VHE) γ-ray, neutrino, and CR observatories, we revisit the possibility of CR production in XRB systems. We focus on the energy budget available for CR acceleration in all Galactic XRB jets and the maximum energy these XRB-CRs could attain, as these are the crucial inputs to determine a potential CR contribution. As mentioned earlier, CRs are deflected in Galactic magnetic field and thus do not point back to their sources. To this end, we also investigate multimessenger possibilities of verifying or falsifying XRB jets as a significant source of CRs.

2 X-RAY BINARY JETS AS COSMIC RAY ACCELERATORS

Active galactic nuclei (AGNs), also powered by accreting black holes (BHs), are natural analogues to XRB jets and their similarities are starting to be quantifiable (Merloni, Heinz & di Matteo 2003; Falcke, Körding & Markoff 2004; McHardy et al. 2006; Plotkin et al. 2012). These systems have the theoretical capability to accelerate ultrahigh-energy CRs (Hillas 1984; Matthews et al. 2019), and we are beginning to see multimessenger hints of extreme particle acceleration occurring either in the jets of AGNs or at the termination shock sites (Pierre Auger Collaboration 2008; HESS Collaboration 2016; IceCube Collaboration 2018). AGN jets are some of the prime candidates of the ultrahigh-energy extragalactic CRs and it is plausible that in the scaled-down XRB jets we might expect similar CR production at lower energies, assuming similar physical processes occur across mass and luminosity scales.

Since their discovery as superluminal sources (Mirabel & Rodríguez 1994), XRB jets have been shown to accelerate leptons to very high energies in the jet-dominated hard state, where high-energy radiation is associated with extremely energetic electrons up to hundreds of TeV. The most characteristic examples are Cygnus X-1 (Zanin et al. 2016), Cygnus X-3 (Tavani et al. 2009), and recently SS 433, which was resolved in the TeV range (HAWC Collaboration 2018; Sudoh, Inoue & Khangulyan 2020). Models of jet emission therefore require very high energy electrons as sources of X-ray and γ-ray emission (e.g. Markoff, Nowak & Wilms 2005; Bosch-Ramon, Romero & Paredes 2006; Zdziarski et al. 2014). Shocks propagating in the jet likely accelerate charged particles to very high energies in a process known as diffusive shock acceleration (Krymskii 1977; Bell 1978), although other acceleration mechanisms such as magnetic reconnection could play a role (Sironi, Petropoulou & Giannios 2015). Such particle acceleration may occur at any point along the jets, and the signature flat/inverted radio spectra suggest that continuous re-acceleration of radiating particles is required throughout the jet to combat adiabatic losses (Blandford & Königl 1979; Malzac 2014; Péault et al. 2019). Some authors have proposed specific zones offset from the BH where this continuous acceleration initiates, such as near the base of the jet, or in a termination shock at jet–interstellar medium (ISM) working surface (Heinz & Sunyaev 2002; Fender, Belloni & Gallo 2004; Markoff et al. 2005; Bordas et al. 2009; Russell et al. 2014; Zdziarski et al. 2014).

Although leptonic processes such as inverse Compton scattering might be the dominant mechanism for such high-energy emission, hadronic particles may also significantly contribute. XRB jets are fed from accretion discs and stellar winds, presumably hadron-rich environments, yet the composition of XRB jets is still unclear. Observational evidence of Doppler shifted atomic line emission at relativistic velocities (Margon et al. 1979; Migliari, Fender & Méndez 2002; Díaz Trigo et al. 2013, 2014) suggests that at least some Galactic XRB jets have hadronic components, but whether this is ubiquitous is unknown. Protons/ions present in the jets will also undergo shock acceleration and in fact would attain much higher energies than electrons due their lower cooling efficiency compared to leptonic counterparts. Some authors suggest proton energies above 10^{15}–10^{16} eV are achievable in XRB jets, considering loss-limited acceleration due to radiative and adiabatic processes (Romero & Vila 2008; Vila & Romero 2011; Pepe, Vila & Romero 2015). If efficient particle acceleration occurs in jets and a hadronic component is present, then a high-energy population of accelerated protons and ions is likely, making XRB jets promising candidate CR sources.

3 POPULATION AND CR POWER OF GALACTIC XRBS

The most important factors when considering generic CR sources are the total available CR power and the maximum attainable CR energy that the source can generate. The former relies on understanding the population and energetics of typical systems. While the latter cannot be directly determined at this time, recent improvements in the modelling of multiwavelength data of XRBs are providing more realistic constraints on cooling rates, and thus potential CR energies. We consider a model for the entire Galactic XRB population, and try to understand the potential total ensemble power. By considering the global energetics and estimating the proportion of power available for CR acceleration, we can estimate the CR flux and evaluate whether XRBs could reasonably account for a significant Galactic CR contribution.

XRBs come in four varieties, categorized by the compact object [either a BH or neutron star (NS)] and the companion star [low mass (LM) or high mass (HM)]. The outflows of each category of system depend strongly on the nature of their accretion. XRBs with LM secondaries accrete via Roche lobe overflow, and thus undergo frequently recurring transient outbursts. Thermal–viscous instabilities developing within the accretion disc give rise to outburst cycles (e.g. Lasota 2001). When observed in the X-ray waveband, an LM-XRB will evolve through a number of distinct accretion states defined by the source spectrum and luminosity (Remillard & McClintock 2006). Comparatively, XRBs with HM secondaries tend to persistently accrete matter via strong stellar winds (with some notable exceptions; see e.g. Tetarenko et al. 2016a) and thus have somewhat more continuous outflows. The initial mass function (IMF; Salpeter 1955; Kroupa 2001) states that LM stars are far more common than HM stars. Therefore, BHs, which generally require more massive progenitors, are less common than NSs. Thus, we expect many more NS-XRBs than BH-XRBs, as well as more systems with LM companions than HM companions. These distributions are encapsulated in population synthesis codes (e.g. Belczynski et al. 2008; Paxton et al. 2011; Spera, Mapelli & Bressan 2015), which use the IMF, stellar evolution, and binary interaction models to predict Galactic population statistics for each type of XRB.

This being said, Fender et al. (2005) suggest that BH-LM-XRBs may actually dominate XRB-CR production despite the fact that they are less numerous in the Galaxy. This stems from the fact that their primarily due to their powerful radio jets implying large amounts of energy available. However, the number of BH-LM-XRBs in the Milky Way is poorly constrained, with population synthesis predictions ranging from 10^2 to 10^5 (e.g. Pfahl, Rappaport & Podsiadlowski 2003; Kiel & Hurley 2006; Yungelson et al. 2006; Sadowski et al. 2008). Unfortunately, the large range of estimates is due to the uncertainties associated with modelling stellar evolution, particularly common envelope and SN kick phases.

The most recent population synthesis results from Olejak et al. (2019) suggest 1.2×10^5 binaries involving a BH and main-sequence star exist in the disc of the Milky Way. However, it is not immediately clear how many of these systems are actively transferring mass and could therefore be classed as XRBs. To understand this, we used the synthetic BH catalogue data base provided by Olejak et al. (2019)[1] to look at all binary systems containing a main-sequence star and a BH. For each of these systems, we looked up the binary separation, a, and approximated the radius of the main-sequence star from its mass. We estimate the proportion of the binaries that are actively transferring mass via Roche lobe overflow by counting only those systems in which the radius of the main-sequence star extends beyond the first Lagrangian point, L_1, of the system. We make use of the fitted formula of Plavec & Kratochvil (1964) for the distance b_1 between L_1 and the centre of the primary:

$$\frac{b_1}{a} = 0.5 - 0.227 \log(q), \tag{1}$$

where q is the binary mass ratio. Given this criterion, we find 5531 XRBs in the model A data sets and 5501 in the model B data sets, where the models differ slightly in the treatment of the common envelope phase. The vast majority of the XRBs are found in the Galactic disc. All the XRBs found in the data sets had main-sequence stars of less than $10\,M_\odot$ and so can be in general considered BH-LM-XRBs.

Table 1. Parameter limits for quantifying CR power of LM companion, BH-XRB systems.

Parameter	Upper	Middle	Lower
A	0.3	0.1	6×10^{-3}
$\frac{L_X}{L_{edd}}$	0.05	0.03	0.01
N	10^4	3×10^3	10^3

Recent observations suggest many more such systems may exist in the Galaxy than previously thought (Corral-Santana et al. 2016; Tetarenko et al. 2016b; Hailey et al. 2018). In particular, based on recent *NuSTAR* observations, Hailey et al. (2018) suggest that 300–1000 BH-LM-XRBs might exist in just the central parsec of the Milky Way, and as such lower estimates from population synthesis simulations may be disfavoured. Given our population synthesis analysis, the density cusp in the Galactic Centre (GC), and the uncertainties involved, we suggest 10^4 is a reasonable upper limit for the Galactic XRB population, as reflected in Table 1. While we take 10^3 as a conservative lower estimate for the total number of Galactic BH-LM-XRBs in this work, we note that only ∼60 BH-XRBs have been (observationally) confirmed to exist in the Galaxy.[2] Thus, the true Galactic BH-LM-XRB population remains a major source of uncertainty in our calculations. Furthermore, XRB outburst durations are typically of the order of months (Tetarenko et al. 2016a), yet CRs take Myr to propagate through the Galaxy. Therefore, predictions made based on current observations make the implicit assumption that the Galactic XRB population has not changed significantly in that time frame.

The fraction of an XRB jet's total power transferred to CR acceleration, the CR luminosity L_{CR}, also involves many parameters lacking strict uncertainties. To estimate the realistic range of values of L_{CR}, we use plausible ranges for each parameter. We adopt the method used in Fender et al. (2005), using an outburst-oriented approach to incorporate advances in recent population studies, particularly the Watchdog data base[3] (Tetarenko et al. 2016a). We simplify our calculations by only considering CR acceleration for BH-LM-XRB systems in the hard, compact jet state,[4] as this is when we expect steady, particle accelerating outflows. By considering only the hard, compact jet state, we can obtain a conservative lower limit

[1] Available at https://bhc.syntheticuniverse.org/.

[2] BlackCat BH-XRB catalogue: http://www.astro.puc.cl/BlackCAT/.

[3] Available at: http://astro.physics.ualberta.ca/WATCHDOG/.

[4] Note that in Tetarenko et al. (2016a), the hard, compact jet state is referred to as the 'hard (Comptonized) state'.

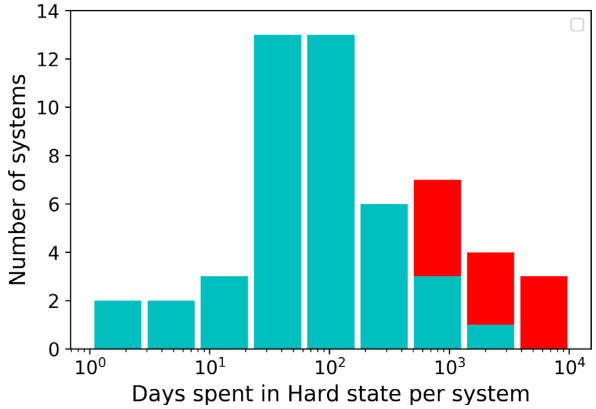

Figure 2. Histogram showing the number of days spent in the hard state for all known BH-XRBs over the entire 19-yr period: in blue transient systems and in red persistent systems (Tetarenko et al. 2016a).

of $L_{\rm CR}$. Realistically, particle acceleration is also expected in other accretion states. In particular, the higher luminosity intermediate state, where transient jets and ejections are observed (e.g. Miller-Jones et al. 2012; Tetarenko et al. 2017; Russell et al. 2019), will likely contribute to $L_{\rm CR}$. However, given the comparatively short lifetime of the intermediate compared to hard accretion states in BH-LM-XRBs (i.e. $t_{\rm IMS} \sim$ 1–10 d, $t_{\rm HS} \sim$ 20–50 d; Tetarenko et al. 2016a), we do not believe the inclusion of the intermediate states will significantly alter our estimate of $L_{\rm CR}$.

The following equation gives us an estimated total power of CRs, in units of the Eddington luminosity, from a set of N similar BH-XRB systems where $M_{\rm BH} = 10\,{\rm M}_{\odot}$:

$$L_{\rm CR} = \frac{1}{2} \cdot \eta \cdot \delta t \cdot A \cdot \left(\frac{L_{\rm X}}{L_{\rm edd}}\right)^{1/2} \cdot N. \quad (2)$$

Here, the factor of 1/2 comes from the fact that we naively assume an equipartition between particles and magnetic fields, as well as sharing of the energy budget between leptons and hadrons. This gives us one-fourth of the available power for hadronic acceleration, multiplied by 2 as there are two similar jets in each system. η is the acceleration efficiency, i.e. how much of the jet power is transferred to high-energy particles via acceleration mechanisms, for which we take a canonical value of 0.1 as supported by simulations (Caprioli & Spitkovsky 2014). As our model is based on outbursts, δt represents the hard state duty cycle of the systems. This factor is the average amount of time a BH-XRB spends in the hard state, the state in which we expect steady, compact jets that efficiently accelerate particles.

To estimate δt, we utilize the data collected in Tetarenko et al. (2016a), in which the authors catalogued X-ray observations of all known BH-XRBs over the last 19 yr. In table 15 of Tetarenko et al. (2016a), we find detailed outburst statistics for 52 systems: 42 classed by the authors as transient, and 10 as persistent. Most pertinent for our study, we find the number of days each system has spent in the hard, compact jet state, which is invaluable to constrain the hard state duty cycle. It is important to note that although almost 25 per cent of all BH-XRBs seem to be persistent accretors with HM companions, this is likely inflated due to observational bias due to their persistent and thus more reliably detected emission. As discussed earlier, HM companions are rarer and live shorter lives, and likely make up a minority of BH-XRB systems.

Of the transient systems, we find mean and median number of days spent in the hard state of 183 and 66 d, respectively (see Fig. 2). Taking the mean and median number of days divided by the total time in which the data were collected (19 yr) as the duty cycle of these systems, we compute hard state duty cycles of 2.6 and 1.0 per cent, respectively. While this data set is the most complete to date with respect to XRB duty cycles, the mean duty cycle derived has to be considered as an upper limit, by virtue of the fact that only systems that have gone into outburst at least once are counted. Furthermore, the average outburst duration (months to years) is still somewhat comparable to the total on-time of 19 yr, which makes rigorous statistical statements difficult.

Lastly, we use the A-parameter normalization prescription, as presented in Fender et al. (2005), to evaluate the XRB jet power from X-ray observations. The A factor depends on both the type of XRB system and accretion state, and the values of A considered in Table 1 are chosen due to the discussion in Fender et al. (2005). By combining (i) the relationship between jet power and radio luminosity motivated by models of steady, conical jets ($L_{\rm radio} \propto L_{\rm J}^{\sim 1.4}$; Blandford & Königl 1979; Falcke & Biermann 1995) and (ii) the observed relation between X-ray and radio luminosity for accreting BH systems ($L_{\rm radio} \propto L_{\rm X}^{0.7}$; Corbel et al. 2000; Merloni et al. 2003; Falcke et al. 2004), Fender et al. (2005) were able to show that jet power ($L_{\rm J}$) depends on the X-ray luminosity, according to

$$L_{\rm J} = A L_{\rm X}^{0.5}. \quad (3)$$

Using an X-ray luminosity of jets varying between 1 and 5 per cent $L_{\rm edd}$ (Maccarone 2003; Miller-Jones et al. 2012; Curran et al. 2014; Russell et al. 2019), the A-parameter normalization estimated by Fender et al. (2005) in this relation (see Table 1), and a mean δt estimated from the Watchdog catalogue as discussed earlier, we are able to compute an $L_{\rm CR}$ estimate via equation (2).

All together, we find a total XRB-CR power in the Milky Way of between approximately 10^{36} and 2×10^{39} erg s^{-1} for the lower and upper bound parameters, respectively, where each XRB provides an average CR power of 10^{33}–10^{36} erg s^{-1} depending on parameter choices. For the reasonable parameter values in the middle column of Table 1, we find $L_{\rm CR} \approx 10^{38}$ erg s^{-1}, approximately 1 per cent of the total estimated Galactic CR power. The actual XRB-CR power output is likely to be significantly higher as we neglect three important additional populations: persistently accreting BH-HM-XRB systems, quiescent systems that are thought to behave much like jet-dominated hard state systems (Plotkin, Gallo & Jonker 2013), and all NS-XRB systems, many of which have powerful jets (Migliari & Fender 2006; Tudose et al. 2006) that may accelerate CRs.

3.1 Constraints from Galactic Centre observations

Galactic CRs propagate from their sources interacting with interstellar gas to produce γ-rays and neutrinos. The observation of diffuse γ-ray emission in a region can therefore tell us about the density of both the ambient medium and high-energy CRs in that region. Furthermore, low-energy CRs interact with molecular clouds to produce X-rays. Observations of such clouds can be used to constrain the low-energy CR flux in the surrounding region. In the following, we look to the inner 200 pc of the Galaxy to constrain the power of Galactic XRB jets as CR sources.

3.1.1 High-energy constraints on the CR power

The recent *NuSTAR* observation by Hailey et al. (2018) suggests the existence of a density cusp of BH-XRBs in the inner parsec of the GC. If this population of BH-XRBs is similar to the broader Galactic population in their potential to accelerate CRs, we expect to see γ-ray signatures of this in the region. Comparing the expected emission

from CR-accelerating XRBs in the GC to the observed emission, we can constrain the CR power of these systems, and thus by extrapolation gain an additional constraint on the Galactic population as a whole. We use the very high energy γ-ray spectra observed by HESS Collaboration (2016), and assume that CRs accelerated in the jets of the *NuSTAR* population of XRBs are responsible for all of the observed γ-rays. This is a very conservative constraint, as we assume all of the γ-ray emission is due to XRB-CR interactions with ambient protons. In reality, it is likely that many sources of CRs, including Sgr A* (HESS Collaboration 2016) and SNe in the region (Jouvin, Lemière & Terrier 2017), and possibly other γ-ray production channels, contribute to the observed HESS flux. In order to estimate the γ-ray emission from a population of cosmic particles injected by a cusp of XRBs located in the inner Galaxy, we perform both an analytical estimate and a numerical simulation.

For the analytical order-of-magnitude estimate, we follow the approach described in detail in Jouvin et al. (2017). The authors consider the well-understood problem of a steady-state injection of hadrons at the GC from GeV all the way up to PeV energies with a single power-law energy spectrum, and their subsequent energy-dependent diffusive escape from a box with a central molecular zone (CMZ) size H. They derive the following expression for the γ-ray luminosity associated with this hadronic population:

$$L_\gamma(>200\,\mathrm{GeV}) = 3.2\times10^{35}\left(\frac{H}{50\,\mathrm{pc}}\right)^2\left(\frac{L_{\mathrm{CR}}}{1.6\times10^{39}\,\mathrm{erg\,s^{-1}}}\right)\times\left(\frac{n}{100\,\mathrm{cm^3}}\right)\ \mathrm{erg\,s^{-1}},$$

where L_{CR} is the total power associated with the CR flux. Given the average gas density in the CMZ and a typical size of the region $H \simeq 100$ pc, we get

$$L_\gamma(>200\,\mathrm{GeV}) = 1.2\times10^{36}\,\mathrm{erg\,s^{-1}}\left(\frac{L_{\mathrm{CR}}}{1.6\times10^{39}\,\mathrm{erg\,s^{-1}}}\right). \quad (4)$$

Given the γ-ray luminosity of the Galactic ridge in $L_\gamma \simeq 3.5\times10^{35}\,\mathrm{erg\,s^{-1}}$ as reported in HESS Collaboration (2016), it is straightforward to compute the maximum allowed power associated with the CR acceleration and injection in the ISM due to the population of the XRBs at the GC, which is still compatible with the HESS measurement. The conservative upper limit on this quantity is $L_{\mathrm{CR}} \sim 10^{38}\,\mathrm{erg\,s^{-1}}$. For more details regarding the analytical estimate, we refer to section 2 in Jouvin et al. (2017).

In order to validate this estimate by means of a numerical simulation, we use the public codes DRAGON (Evoli et al. 2017) and GAMMASKY. Using these codes, we are able to propagate CRs from any given source distribution and, adopting detailed models for the gas and interstellar radiation in the Galaxy, compute the γ-ray/neutrino flux associated with the CR population under consideration. We set up the DRAGON code to inject CRs with a Gaussian source term centred on the GC with a 1 pc width, consistent with the Hailey et al. (2018) population. We set a hard injection spectrum described by a single power law $Q = Q_0(E/E_0)^{-\alpha}$, with $\alpha = 2.2$ and $E_{\mathrm{min}} = 1$ GeV, and let the particles propagate through the CMZ and diffuse out of the Galaxy.

After the equilibrium distribution of CRs is obtained, we compute the hadronic γ-ray flux from the Galactic ridge region with the GAMMASKY code, adopting the same model for the gas distribution in the CMZ as in Gaggero et al. (2017). For a CR injected power $L_{\mathrm{CR}}(>1\,\mathrm{GeV}) \simeq 10^{38}\,\mathrm{erg\,s^{-1}}$, we obtain an average flux from the Galactic ridge region $\mathrm{d}\Phi/\mathrm{d}E_\gamma = 2\times10^{-11}\,\mathrm{GeV^{-1}\,cm^{-2}\,s^{-1}\,sr^{-1}}$ at 1 TeV (see Aharonian et al. 2006). Furthermore, we obtain an integrated flux of $\mathrm{d}\Phi/\mathrm{d}E_\gamma \simeq 2\times10^{-12}\,\mathrm{TeV^{-1}\,cm^{-2}\,s^{-1}}$ at 1 TeV from the inner annulus centred on Sgr A* as considered in HESS Collaboration (2016). Such γ-ray flux clearly saturates the γ-ray emission reported by the HESS Collaboration (see Fig. 3); thus, we confirm the analytical order-of-magnitude estimate for the upper limit on the power injected in CRs at the GC from an XRB population.

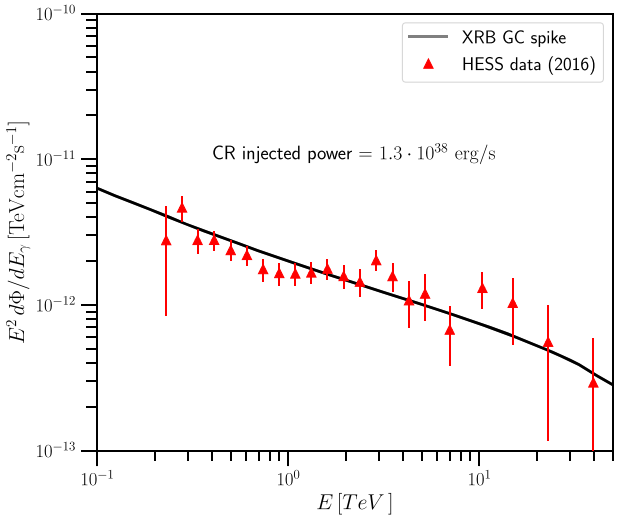

Figure 3. γ-ray spectral energy distribution associated with the population of CRs accelerated by XRBs located at the GC. We have assumed a CR injected power $L_{\mathrm{CR}}(>1\,\mathrm{GeV}) = 1.3\times10^{38}\,\mathrm{erg\,s^{-1}}$. The γ-ray flux is integrated over the region of interest defined in figs 1 and 3 of HESS Collaboration (2016); the HESS data are shown as red triangles.

Hailey et al. (2018) suggest that between 300 and 1000 BH-XRBs exist in the GC. Although these systems currently seem to be mostly in quiescence, they could have been more active in the past. If we conservatively assume that CR acceleration in the jets of these systems is responsible for all of the observed γ-ray flux in HESS Collaboration (2016), we can constrain the maximum CR power per system to be $10^{34} \lesssim L_{\mathrm{CR}} \lesssim 3\times10^{35}\,\mathrm{erg\,s^{-1}}$. Extrapolating this to the wider Galactic population of 10^3–10^4 systems, we find a total XRB-CR power of 10^{37} to $3\times10^{39}\,\mathrm{erg\,s^{-1}}$. This range of values falls within our estimates for the total XRB-CR power as found earlier, representing 0.1–10 per cent of the total Galactic CR power. This is consistent with our total XRB-CR power derived earlier in this section. We stress that this is an upper limit based on the entire γ-ray flux as observed by HESS Collaboration (2016) to originate from CRs accelerated in jets of the density cusp of XRBs in the GC, and is primarily used as a sanity check to ensure our assumptions do not violate observational limits.

3.1.2 Low-energy constraints on the CR power

An additional constraint on the CR power in the GC region comes from X-ray observations of the giant molecular clouds in the CMZ. Once again, this is an upper limit as we assume XRB-CRs from the Hailey et al. (2018) population are the only sources of CRs that contribute to the X-ray illumination.

GeV CR protons/ions bombarding giant molecular clouds produce X-ray emission through collisional ionization and bremsstrahlung. The GC molecular cloud Sgr B2's X-ray emission has been decaying over the last two decades, which is primarily due to X-ray echo of past activities of Sgr A* (Inui et al. 2009; Terrier et al. 2010; Dogiel et al. 2011). However, in the recent years, as the X-ray echo component

further faded away, Sgr B2's X-ray emission seemed to enter a constant low-flux stage, which is interpreted as GeV CR illumination. Observations of the Sgr B2 molecular cloud using *NuSTAR* in 2013 have shown that, after more than 10 yr of flux decaying, the remaining X-ray emission from Sgr B2 is consistent with the GeV CR illumination scenario (Zhang et al. 2015). Assuming that all the Sgr B2 X-ray emission comes from CR illumination, Zhang et al. (2015) derived a CR proton spectral index of $\alpha = 1.9^{+0.8}_{-0.7}$ and a required GeV proton power of $L_{\rm CR} = (0.4\text{–}2.3) \times 10^{39}$ erg s^{-1}. We note that the GeV proton power derived from this method shall be taken as an upper limit, since the X-ray emission from Sgr B2 in 2013 can come partly from CR illumination, and partly from X-ray echoes. Future Sgr B2 X-ray observations will put a tighter constraints on the required CR proton power in the CMZ. This CR power upper limit from X-ray observation of Sgr B2 is consistent with the new estimate of XRB-CR power of the Hailey et al. (2018) population derived in this work.

3.1.3 *Consistency of constraints*

As we have both low-energy and high-energy constraints on the CR power in the region, we can check whether they are compatible by assuming our XRB-CR injection spectral index of $\alpha = 2.2$ holds across the entire energy range. The total low-energy CR power upper limit of $(0.4\text{–}2.3) \times 10^{39}$ erg s^{-1} applies to CR energies between $E_{\rm min} = 1$–100 MeV and $E_{\rm max} = 1$ GeV, i.e. the model parameters used by Zhang et al. (2015). Using this, we extrapolate to find an allowed high-energy XRB-CR power due to the Hailey et al. (2018) population of $L_{\rm CR}(>1\ {\rm GeV}) \leq (1.3\text{–}39) \times 10^{38}$ erg s^{-1}, where the range of values reflects the allowed ranges of both the $E_{\rm min}$ parameter and low-energy CR power constraints described in Section 3.1.2. As the analytical and numerical analysis of the HESS data suggests an upper limit of $L_{\rm CR}(>1\ {\rm GeV}) \sim 10^{38}$ erg s^{-1}, we find that the HESS γ-ray measurements better constrain the CR power in the region, assuming $\alpha = 2.2$. However, softer CR injection spectra or alternative contributions to the observed γ-rays in region would mean the low-energy constraints are more stringent limits.

4 MAXIMUM ENERGY OF XRB-CRS

We have shown that BH-XRBs can viably contribute a significant fraction of the total Galactic CR power without violating constraints in the GC, so we now consider the maximum energy attainable by XRB-CRs.

The maximum energy of accelerated CRs in jets is limited either by energy losses (synchrotron, inverse Compton, and adiabatic losses are the primary channels) or by the Hillas criteria for confinement (Hillas 1984). This is to say that accelerated CRs must stay confined within the accelerating medium in order to undergo re-acceleration, which we can quantify using the Larmor radius. The importance of the radiative losses can be quantified by comparing the time-scales of the loss channels and the time-scale of the acceleration mechanism. We compute the maximum energy as a function of jet height, $E_{\rm max}(z)$, such that it satisfies both of these constraints. Here, we neglect proton–photon interactions. These interactions are expected to be subdominant at these extreme energies and magnetic field strengths even in photon-rich XRB systems (Romero & Vila 2008; Pepe et al. 2015; Sudoh et al. 2020). This is especially true for BH-LM-XRB systems where the LM companions are expected to have relatively modest photon field contributions.

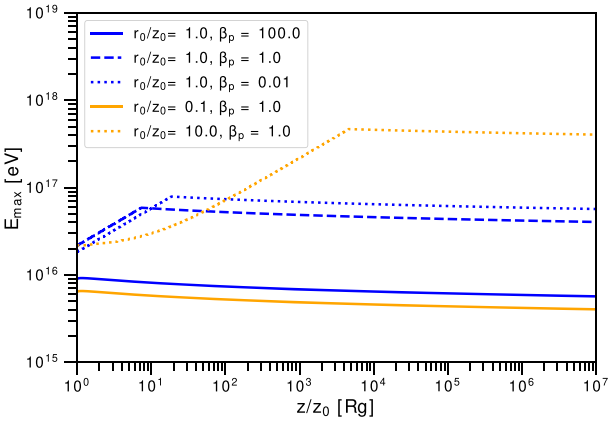

Figure 4. Maximum proton energy as a function of distance from the base of the jets for a quasi-isothermal jet model, where we use $\eta = 0.1$. We vary two important parameters: initial aspect ratio r_0/z_0 in orange and plasma $\beta_{\rm p} = U_{\rm e+p}/U_{\rm B}$ in blue. The higher the initial aspect ratio, the wider the jet, and thus the particles are confined more easily at high jet heights; the smaller the $\beta_{\rm p}$ value, the higher the magnetic field strength, which results in smaller Larmor radii, aiding confinement, but producing larger synchrotron losses. In general, the maximum energy is limited by radiative losses at lower jet height due to strong magnetic fields, and is confinement limited at large z.

4.1 Jet model

We calculate the maximum energy of accelerated protons for the three different dynamical jet models (isothermal, adiabatic, and quasi-isothermal *agnjet* variant) outlined in Crumley et al. (2017). In Appendix A, we provide an overview of the different jet models and the parameters involved in computing the maximum CR energy. In Fig. 4, we focus on the quasi-isothermal model as used in the *agnjet* model, due to its ability to fit the flat jet spectrum we see in multiwavelength XRB data (Markoff, Falcke & Fender 2001; Markoff et al. 2005).

In general, models of jets are based on the jet–disc symbiosis ansatz laid out in Falcke & Biermann (1995). The jet is fed by the disc and the power of the jet at a height z is given by

$$L_{\rm j}(z) = \Gamma_{\rm j}^2 \beta_{\rm j} c \omega \pi z^2 \sin^2(\theta), \tag{5}$$

where $\Gamma_{\rm j}(z)$ is the Lorentz factor of the bulk jet flow, z is the height of the jet above the BH (z_0 is the height of the jet base), and $\omega(z)$ is the enthalpy. For a jet with a co-moving particle number density, $n(z)$, the enthalpy can be written as

$$\omega(z) = nmc^2 + U_{\rm j} + P_{\rm j}. \tag{6}$$

Here, $U_{\rm j}$ and P_j are the energy density and the pressure of the jet, respectively. We can approximate to

$$\omega(z) = nm_{\rm p}c^2 + \Gamma_{\rm adi} U_{\rm j}, \tag{7}$$

where we have assumed the jet can be treated as an ideal gas with adiabatic index, $\Gamma_{\rm adi}$, as in Falcke & Biermann (1995). These equations are valid for all jet models considered in Appendix A.

To compute radiative losses and confinement of accelerated CRs in the jet, the most important parameters are the jet radius, $R(z)$, and the magnetic field strength, $B(z)$. In all models, we define the magnetic field strength of the jet as

$$B(z) = \sqrt{\frac{8\pi U_{\rm j}(z)}{\beta_{\rm p} + 1}}, \tag{8}$$

where

$$\beta_{\rm p} = \frac{U_{\rm e+p}}{U_{\rm B}}. \tag{9}$$

$\beta_{\rm p}$ is an important free parameter that sets how energy is distributed among particles and magnetic fields, and we show how different values of $\beta_{\rm p}$ affect the maximum CR energy in Fig. 4.

The prescription of $U_{\rm j}(z)$ depends on the choice of jet model as shown in Appendix A. From equations (5)–(7), we see that the value of $L_{\rm j}(z_0)$, the power at the base of the jet, depends on $n(z_0)$ and $U_{\rm j}(z_0)$, the number density and internal energy density at the base of the jet. In this analysis, we normalize $L_{\rm j}(z_0)$ to the hard state jet power expected from the discussion in the previous section: $\sim$1–5 per cent of the Eddington luminosity of a 10 $M_\odot$ BH. This results in a jet base magnetic field strength, $B(z_0)$, of (5–10) $\times$ 10^6 G, in line with other models (Romero & Vila 2008; Pepe et al. 2015).

To compute the radius of the jet, we follow Crumley et al. (2017). For the isothermal and adiabatic jet models, we use a simple conical jet model in which

$$r_{\rm cone}(z) = r_0 + (z - z_0)\sin(\theta). \tag{10}$$

Here, θ is the opening angle of the jet. This means that r_0 is an important free geometric parameter, which sets the initial radius of the jet. It directly influences the extent to which high-energy CRs can be confined, resulting in further acceleration. The quasi-isothermal *agnjet* model used in Fig. 4 is not a conical model but instead considers self-collimation. This results in a slightly different jet radius profile:

$$r_{\rm coll}(z) = r_0 + (z - z_0)\frac{\gamma_0\beta_0}{\gamma_{\rm j}\beta_{\rm j}}. \tag{11}$$

This gives us a slightly narrower jet for larger values of z.

When we calculate the maximum energy of accelerated CRs in the jet, we vary both r_0 and $\beta_{\rm p}$. This helps us understand the parameter space available for a generic XRB population, and the different maximum CR energies attainable. As the magnetic field strength depends strongly upon the internal energy density of the jet, $U_{\rm j}$, the maximum CR energy increases significantly for higher jet powers. This is to say that the most powerful XRB jets may be capable of producing higher energy CRs than outlined here. For more on the jet models, please see Appendix A.

4.2 Calculating maximum energy

The time-scales of interest in computing the maximum energy are as follows:

$$t_{\rm acc}^{-1} = \frac{\eta e c B}{E}, \tag{12}$$

$$t_{\rm sync}^{-1} = \frac{4}{3}\left(\frac{m_{\rm e}}{m_{\rm p}}\right)^3 \frac{c\,\sigma_{\rm T}\,U_{\rm B}}{m_{\rm e}c^2}\frac{E}{m_{\rm p}c^2}, \tag{13}$$

$$t_{\rm adi}^{-1} = \frac{2}{3}\frac{\beta}{z}. \tag{14}$$

The maximum CR energy, as limited by radiation losses, is given by the following condition:

$$t_{\rm acc}(E,z)^{-1} > t_{\rm adi}(E,z)^{-1} + t_{\rm sync}(E,z)^{-1}. \tag{15}$$

The condition for confinement can be rewritten from Hillas' seminal paper (Hillas 1984) as

$$E_{\rm CR}(z) < \frac{B(z)}{\mu{\rm G}} \times \frac{R(z)}{\rm pc} \times \frac{\beta}{0.5} \times 10^{15}\,{\rm eV}. \tag{16}$$

Equations (15) and (16) provide us with the constraints with which we compute the maximum jet power for all models. Specifically, we compute the maximum CR energy limited by each of these constraints, and take the minimum of these two values. In Fig. 4, we show our results for how the maximum possible energy varies as a function of the jet height for the quasi-isothermal jet model (that provides the best description of flat spectra jets; Crumley et al. 2017), for different values of the initial aspect ratio, r_0/z_0, and $\beta_{\rm p}$ of the jet.

Radiative losses dominate near the BH, as the high magnetic field strength close to the base of the jet results in large synchrotron losses. Most models then show a flattening when a lack of confinement of the particles limits the maximum energy of XRB-CR higher up in the jet. One can assume that in the confinement-limited region, accelerated CRs that exceed the critical energy at which the particle stays confined escape the jet to propagate through the ISM.

We find that the maximum attainable CR energy depends strongly on geometry, jet model, and acceleration region, but in general protons can reach energies of 10^{16}–10^{17} eV if accelerated with a canonical efficiency of $\eta = 0.1$ (Caprioli & Spitkovsky 2014). We note that varying η scales the maximum energy linearly in the radiative loss-dominated regime at small z. These calculations assume protons (i.e. $Z = 1$), but if more massive CR ions are present in the jet they would attain greater energies as the maximum CR energy scales with rigidity. Lastly, we note that in specific geometries and acceleration regions CR energies higher than 10^{17} eV could be reached, but this might only be plausible in atypical systems such as very powerful, wide, or highly magnetized jets.

5 MULTIMESSENGER TESTS OF THE XRB-CR SCENARIO

Any source class contribution to the CR spectrum can only be directly probed by CR observatories if those sources dominate the spectrum at specific energies. Although XRB-CRs might dominate the parts of the CR spectrum, this is highly dependent on the total CR power, maximum energy of individual CRs, and the acceleration power-law index. Given our results, we suggest that in the most optimistic case XRB-CRs might dominate (or contribute significantly to) the spectrum close to 10^{17} eV, near the second knee, where a light-mass component has been detected (Pierre Auger Collaboration 2014; Buitink et al. 2016; Hanlon 2019; Yushkov 2019).

The latest results from CR instruments seem to only strengthen the evidence for a light-mass component above 10^{17} eV (Kang 2019; Yushkov 2019), and upgrades of such instruments (e.g. Pierre Auger Collaboration 2016; Mulrey et al. 2019) will be crucial to understand the composition of the transitional energy region between Galactic and extragalactic CRs. While this observed lighter mass component could be interpreted as the start of the extragalactic component, this would require the ankle to be a propagation effect. Thus, any Galactic CR accelerator able to reach these energies is of great interest. However, the allowed range of XRB-CR power found in this work means that the contribution could be subdominant at all energy ranges, and thus any confirmation of CR acceleration in XRB jets might only be found via indirect measurements of γ-rays or neutrinos. In Fig. 1, we show a schematic of the all-particle CR spectrum, with a range of allowed contributions from the XRB-CR component calculated in this work. In particular, we show (green dashed line) the maximum allowed contribution, which is calculated by taking the upper parameters in Table 1. Such a contribution would make up a significant fraction of the CRs in the energy range between second knee and ankle, where the role of a second Galactic component is currently under debate.

5.1 γ-rays

Several XRB jets are now known to emit γ-rays (Tavani et al. 2009; Bordas et al. 2015; Zanin et al. 2016; HAWC Collaboration 2018), although some observations have reported non-detections (Bodaghee et al. 2013; Ahnen et al. 2017a; MAGIC Collaboration 2018). Given the transient nature of some of these sources (and especially the complex environment of the SS 433 system), we do not necessarily expect CR acceleration and subsequent γ-ray emission continuously from XRB systems. Furthermore, although the observation of such high-energy radiation is a clear signature of particle acceleration, it is not trivial to pin down the origin of observed γ-rays that could be leptonic, hadronic, or a combination. The upcoming, next-generation Cherenkov Telescope Array (CTA; Cherenkov Telescope Array Consortium 2019) will have an order of magnitude better sensitivity compared to current facilities, and up to four to five orders of magnitude better sensitivity than *Fermi* in the 100 GeV range for fast transients. CTA will thus likely be able to detect and identify the Galactic PeV BH-XRB sources in the near future (Kantzas et al., in preparation).

As a consistency check, we again used the DRAGON code to look at the expected diffuse Galactic γ-ray emission due to the XRB population. However, as this population is subdominant to the (SNR) low-energy CR sources below 10^{16} eV, it is impossible to distinguish the sources in currently observable γ-ray wavelengths. Therefore, we suggest point source γ-ray observations of the most powerful XRB jets will pave the way for identifying CRs from XRBs through traditional electromagnetic observations.

5.2 Neutrinos

Neutrinos are also produced through CR interactions with protons or photons, and XRB jets have long been predicted as a sources of neutrinos (Levinson & Waxman 2001; Distefano et al. 2002). As neutrino astronomy is still in its infancy, observations of Galactic-origin neutrinos thus far have been compatible with background (Albert et al. 2017). However, the current limits from a joint analysis of ANTARES and IceCube data (Albert et al. 2018) are now getting close to the most optimistic predictions regarding the expected Galactic neutrino flux. Therefore, the clear detection of a component associated with the Galactic plane may be round the corner (see for instance, a recent 2σ hint reported in Aartsen et al. 2019), and diffuse Galactic searches could provide indeed a novel approach towards identifying a second source of Galactic CRs. Neutrino observations probe higher energies than γ-ray facilities and therefore high-energy breaks in the diffuse Galactic neutrino spectra (Aartsen et al. 2017; Albert et al. 2018) could be interpreted as separate contributions from different CR source classes.

Using the DRAGON code, we compute the expected diffuse neutrino emission due to CRs propagating from two different components: the dominant low-energy (SNR) component and a higher energy (XRB) component. We assume a low-energy component that saturates the observed CR spectrum below the knee, as expected by the dominant Galactic CR source. The subdominant, higher maximum energy component has approximately 10 per cent of the power of the low-energy source, in agreement with most optimistic findings of total XRB-CR power in Section 3. For the source distributions, we have assumed a Lorimer pulsar distribution (Lorimer et al. 2006) for both source populations, as this is a good approximate tracer of compact objects and therefore of SNRs and XRBs. In Fig. 5, we see the resulting diffuse neutrino spectra due to these two components, where we assume the low-energy and higher energy components are due

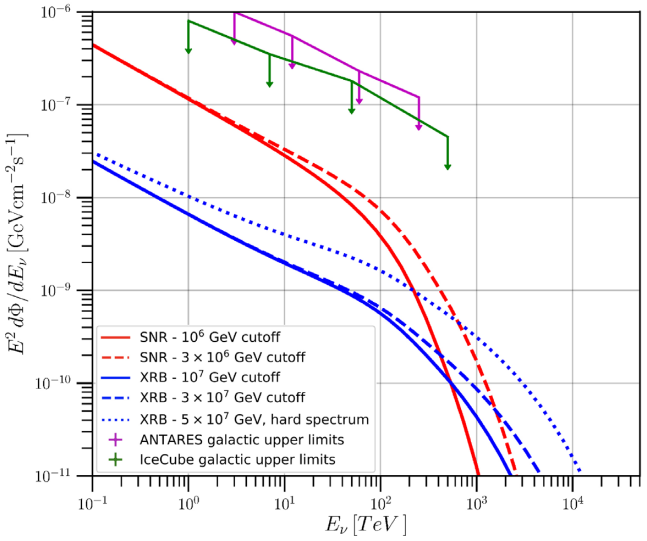

Figure 5. The predicted diffuse Galactic neutrino spectrum from SNR-CRs and XRB-CRs with joint upper limits from ANTARES and IceCube (Aartsen et al. 2017) using the DRAGON code. Specifically, we note that breaks in the spectra are predicted in the total spectrum at model-dependent sensitivities even with very conservative maximum energy cut-offs.

to SNR and XRB sources, respectively. We plot different maximum energy cut-offs, as the maximum CR energy for each source is not well known. Unlike CRs, neutrinos trace back to their sources and thus confirming a break/hardening in the spectrum towards the Milky Way could verify the Galactic origin of high-energy CRs. The current upper limits on the Galactic contribution to the astrophysical neutrino flux by IceCube and ANTARES are also shown in the figure.

As the next generation of neutrino observatories come online (Icecube-Gen2, IceCube-Gen2 Collaboration 2014; KM3-NET (2.0), Adrián-Martínez et al. 2016), we can probe PeV energy ranges in order to verify whether there are two clear populations of high-energy CR sources within our Galaxy. As diffuse neutrino limits are already encroaching on best models of neutrino emission from Galactic CRs, the 10-fold detector volume increase specified for IceCube-Gen2 will probe our predictions of a break in the Galactic neutrino spectrum due to a high-energy Galactic component. Furthermore, KM3-NET upgrades over the next decade will increase the angular resolution of detections to $<0.1^\circ$ at PeV energies. Coupled with greater sensitivities, point source neutrino astronomy will soon be at the forefront of identifying CR sources within our Galaxy. Once these upgrades are realized, XRB systems such as Cygnus X-1 will be key targets for neutrino observatories to test whether XRB jets are important CR accelerators.

6 CONCLUSION

We have suggested that XRB jets could accelerate protons to high energies, similar to their larger counterparts in AGNs. Within the uncertainties allowed by current population models, jet composition, and GC observational constraints, a total XRB-CR power of between 10^{36} and 10^{39} erg s^{-1} is possible. The most likely allowed value of around 10^{38} erg s^{-1} means XRB-CRs could contribute a few per cent of the dominant SNR-CR component, representing a non-negligible contribution to the observed CR spectrum. The maximum energy of XRB-CR is relatively high compared to other Galactic sources of CRs, with models suggesting protons could be accelerated to 10^{16}–10^{17} eV in some systems. Together these two results indicate

that XRB-CRs could even dominate the total CR spectrum in part of the transition region between SNR-CR and extragalactic CR components, above the knee and below the ankle, in broad agreement with recent mass composition results. Lastly, we suggest multimessenger possibilities to confirm XRB-CR (or generic second Galactic components) through diffuse neutrino and γ-ray measurements of our Galaxy, as well as point source observations.

ACKNOWLEDGEMENTS

We would like to thank R. Bartels, S. Gabici, D. Kantzas, and B. Tetarenko for helpful discussions. We would also like to thank the anonymous referee for their thorough and insightful comments that improved this work. AJC was partially supported by the Netherlands Research School for Astronomy (NOVA). The work of DG has received financial support through the Postdoctoral Junior Leader Fellowship Programme from "la Caixa" Foundation (grant no. LCF/BQ/LI18/11630014). DG was also supported by the Spanish Agencia Estatal de Investigación through the grants PGC2018-095161-B-I00, IFT Centro de Excelencia Severo Ochoa SEV-2016-0597, and Red Consolider MultiDark FPA2017-90566-REDC. SM was supported by an NWO (Netherlands Organisation for Scientific Research) VICI award, grant no. 639.043.513.

REFERENCES

Aartsen M. G. et al., 2017, ApJ, 849, 67
Aartsen M. G. et al., 2019, ApJ, 886, 12
Ackermann M. et al., 2013, Science, 339, 807
Adrián-Martínez S. et al., 2016, J. Phys. G: Nucl. Phys., 43, 084001
Aharonian F. et al., 2006, Nature, 439, 695
Ahnen M. L. et al., 2017a, MNRAS, 471, 1688
Ahnen M. L. et al., 2017b, MNRAS, 472, 2956
Albert A. et al., 2017, J. Cosmol. Astropart. Phys., 2017, 019
Albert A. et al., 2018, ApJ, 868, L20
Belczynski K., Kalogera V., Rasio F. A., Taam R. E., Zezas A., Bulik T., Maccarone T. J., Ivanova N., 2008, ApJS, 174, 223
Bell A. R., 1978, MNRAS, 182, 147
Berezinsky V. S., Bulanov S. V., Dogiel V. A., Ptuskin V. S., 1990, in Ginzburg V. L., ed., Astrophysics of Cosmic Rays. North-Holland, Amsterdam
Blandford R. D., Königl A., 1979, ApJ, 232, 34
Blasi P., 2013, A&AR, 21, 70
Bodaghee A., Tomsick J. A., Pottschmidt K., Rodriguez J., Wilms J., Pooley G. G., 2013, ApJ, 775, 98
Bordas P., Bosch-Ramon V., Paredes J. M., Perucho M., 2009, A&A, 497, 325
Bordas P., Yang R., Kafexhiu E., Aharonian F., 2015, ApJ, 807, L8
Bosch-Ramon V., Romero G. E., Paredes J. M., 2006, A&A, 447, 263
Buitink S. et al., 2016, Nature, 531, 70
Caprioli D., Spitkovsky A., 2014, ApJ, 783, 91
Cherenkov Telescope Array Consortium, 2019, Science with the Cherenkov Telescope Array. World Scientific Press, Singapore
Corbel S., Fender R. P., Tzioumis A. K., Nowak M., McIntyre V., Durouchoux P., Sood R., 2000, A&A, 359, 251
Corral-Santana J. M., Casares J., Muñoz-Darias T., Bauer F. E., Martínez-Pais I. G., Russell D. M., 2016, A&A, 587, A61
Crumley P., Ceccobello C., Connors R. M. T., Cavecchi Y., 2017, A&A, 601, A87
Curran P. A. et al., 2014, MNRAS, 437, 3265
Díaz Trigo M., Miller-Jones J. C. A., Migliari S., Broderick J. W., Tzioumis T., 2013, Nature, 504, 260
Díaz Trigo M., Migliari S., Miller-Jones J. C. A., Guainazzi M., 2014, A&A, 571, A76
Distefano C., Guetta D., Waxman E., Levinson A., 2002, ApJ, 575, 378
Dogiel V., Chernyshov D., Koyama K., Nobukawa M., Cheng K.-S., 2011, PASJ, 63, 535
Evoli C., Gaggero D., Vittino A., Di Bernardo G., Di Mauro M., Ligorini A., Ullio P., Grasso D., 2017, J. Cosmol. Astropart. Phys., 2017, 015
Falcke H., Biermann P. L., 1995, A&A, 293, 665
Falcke H., Körding E., Markoff S., 2004, A&A, 414, 895
Fang K., Kotera K., Olinto A., 2013, in APS Meeting Abstracts. p. L14.001
Fender R. P., Belloni T. M., Gallo E., 2004, MNRAS, 355, 1105
Fender R. P., Maccarone T. J., van Kesteren Z., 2005, MNRAS, 360, 1085
Gabici S., Gaggero D., Zandanel F., 2016, preprint (arXiv:1610.07638)
Gaggero D., Grasso D., Marinelli A., Taoso M., Urbano A., 2017, Phys. Rev. Lett., 119, 031101
Gaisser T. K., Stanev T., Tilav S., 2013, Front. Phys., 8, 748
Giacinti G., Kachelrieß M., Semikoz D. V., 2015, Phys. Rev. D, 91, 083009
Ginzburg V. L., Syrovatskii S. I., 1964, The Origin of Cosmic Rays. Macmillan, New York
Hailey C. J., Mori K., Bauer F. E., Berkowitz M. E., Hong J., Hord B. J., 2018, Nature, 556, 70
Hanlon W., 2019, Proc. 36th Int. Cosm. Ray Conf. (ICRC 2019), 280
HAWC Collaboration, 2018, preprint (arXiv:1810.01892)
Heinz S., Sunyaev R., 2002, A&A, 390, 751
HESS Collaboration, 2016, Nature, 531, 476
Hillas A. M., 1984, ARA&A, 22, 425
Hillas A. M., 2005, J. Phys. G: Nucl. Phys., 31, R95
IceCube Collaboration, 2018, Science, 361, 147
IceCube-Gen2 Collaboration, 2014, preprint (arXiv:1412.5106)
Inui T., Koyama K., Matsumoto H., Tsuru T. G., 2009, PASJ, 61, S241
Jokipii J. R., Morfill G., 1987, ApJ, 312, 170
Jouvin L., Lemière A., Terrier R., 2017, MNRAS, 467, 4622
Kampert K.-H., Unger M., 2012, Astropart. Phys., 35, 660
Kang D., 2019, Proc. 36th Int. Cosm. Ray Conf. (ICRC 2019), 306
Kiel P. D., Hurley J. R., 2006, MNRAS, 369, 1152
Kroupa P., 2001, MNRAS, 322, 231
Krymskii G. F., 1977, Akad. Nauk SSSR Dokl., 234, 1306
Lasota J.-P., 2001, New Astron. Rev., 45, 449
Levinson A., Eichler D., 1993, ApJ, 418, 386
Levinson A., Waxman E., 2001, Phys. Rev. Lett., 87, 171101
Lorimer D. R. et al., 2006, MNRAS, 372, 777
Maccarone T. J., 2003, A&A, 409, 697
McHardy I. M., Koerding E., Knigge C., Uttley P., Fender R. P., 2006, Nature, 444, 730
MAGIC Collaboration, 2018, A&A, 612, A14
Malzac J., 2014, MNRAS, 443, 299
Margon B., Ford H. C., Grandi S. A., Stone R. P. S., 1979, ApJ, 233, L63
Markoff S., Falcke H., Fender R., 2001, A&A, 372, L25
Markoff S., Nowak M. A., Wilms J., 2005, ApJ, 635, 1203
Matthews J. H., Bell A. R., Blundell K. M., Araudo A. T., 2019, MNRAS, 482, 4303
Merloni A., Heinz S., di Matteo T., 2003, MNRAS, 345, 1057
Migliari S., Fender R. P., 2006, MNRAS, 366, 79
Migliari S., Fender R., Méndez M., 2002, Science, 297, 1673
Miller-Jones J. C. A. et al., 2012, MNRAS, 421, 468
Mirabel I. F., Rodríguez L. F., 1994, Nature, 371, 46
Mulrey K. et al., 2019, Proc. 36th Int. Cosm. Ray Conf. (ICRC 2019), 363
Olejak A., Belczynski K., Bulik T., Sobolewska M., 2019, preprint (arXiv:1908.08775)
Paxton B., Bildsten L., Dotter A., Herwig F., Lesaffre P., Timmes F., 2011, ApJS, 192, 3
Péault M. et al., 2019, MNRAS, 482, 2447
Pepe C., Vila G. S., Romero G. E., 2015, A&A, 584, A95
Peters B., 1961, Il Nuovo Cimento, 22, 800
Pfahl E., Rappaport S., Podsiadlowski P., 2003, ApJ, 597, 1036
Pierre Auger Collaboration, 2008, Astropart. Phys., 29, 188
Pierre Auger Collaboration, 2014, preprint (arXiv:1409.5083)
Pierre Auger Collaboration, 2016, preprint (arXiv:1604.03637)
Plavec M., Kratochvil P., 1964, Bull. Astron. Inst. Czech., 15, 165
Plotkin R. M., Markoff S., Kelly B. C., Körding E., Anderson S. F., 2012, MNRAS, 419, 267

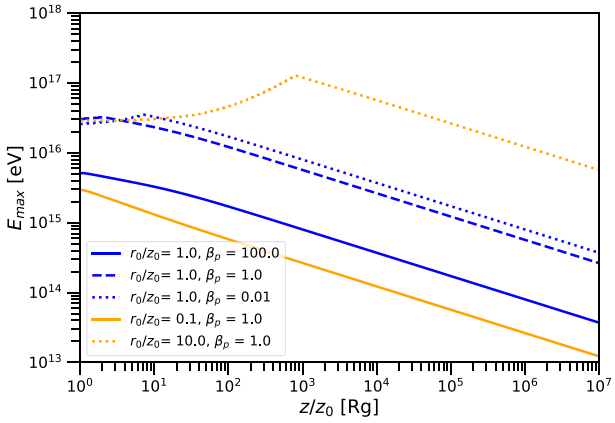

Figure A1. Maximum CR energy as a function of jet height z for the adiabatic jet model.

Plotkin R. M., Gallo E., Jonker P. G., 2013, ApJ, 773, 59
Remillard R. A., McClintock J. E., 2006, ARA&A, 44, 49
Romero G. E., Vila G. S., 2008, A&A, 485, 623
Russell T. D., Soria R., Miller-Jones J. C. A., Curran P. A., Markoff S., Russell D. M., Sivakoff G. R., 2014, MNRAS, 439, 1390
Russell T. D. et al., 2019, ApJ, 883, 198
Sadowski A., Ziółkowski J., Belczyński K., Bulik T., 2008, in Bandyopadhyay R. M., Wachter S., Gelino D., Gelino C. R., eds, AIP Conf. Proc. Vol. 1010, A Population Explosion: The Nature & Evolution of X-Ray Binaries in Diverse Environments. Am. Inst. Phys., New York, p. 404
Salpeter E. E., 1955, ApJ, 121, 161
Sironi L., Petropoulou M., Giannios D., 2015, MNRAS, 450, 183
Spera M., Mapelli M., Bressan A., 2015, MNRAS, 451, 4086
Sudoh T., Inoue Y., Khangulyan D., 2020, ApJ, 889, 146
Tavani M. et al., 2009, Nature, 462, 620
Terrier R. et al., 2010, ApJ, 719, 143
Tetarenko B., Sivakoff G., Heinke C., Gladstone J., 2016a, ApJS, 222, 15
Tetarenko B. E. et al., 2016b, ApJ, 825, 10
Tetarenko A. J. et al., 2017, MNRAS, 469, 3141
Thoudam S., Rachen J. P., van Vliet A., Achterberg A., Buitink S., Falcke H., Hörandel J. R., 2016, A&A, 595, A33
Tudose V., Fender R. P., Kaiser C. R., Tzioumis A. K., van der Klis M., Spencer R. E., 2006, MNRAS, 372, 417
Vila G. S., Romero G. E., 2011, preprint (arXiv:1104.2071)
Vink J., Laming J. M., 2003, ApJ, 584, 758
Yungelson L. R., Lasota J.-P., Nelemans G., Dubus G., van den Heuvel E. P. J., Dewi J., Portegies Zwart S., 2006, A&A, 454, 559
Yushkov A., 2019, 36th Int. Cosm. Ray Conf. (ICRC 2019), 482
Zanin R., Fernández-Barral A., de Oña Wilhelmi E., Aharonian F., Blanch O., Bosch-Ramon V., Galindo D., 2016, A&A, 596, A55
Zdziarski A. A., Pjanka P., Sikora M., Stawarz Ł., 2014, MNRAS, 442, 3243
Zhang S. et al., 2015, ApJ, 815, 132

APPENDIX

In Section 4, we looked at dynamical jet models in order to estimate the maximum attainable CR energy as a function of jet height. We rely heavily on Crumley et al. (2017), in which the equations governing the different jet models are derived. Here, we give a quick overview of each jet model, and show how the maximum CR energy depends on the jet model. As mentioned in Section 4, we believe that for XRB jets, the quasi-isothermal jet model is the most appropriate.

From this starting point, assumptions about the physics of the jet lead to different models. The most important difference is that in the adiabatic jet model, adiabatic losses are not compensated for. In all other models, losses are compensated for by continuous re-acceleration of particles. In the isothermal model, adiabatic losses are fully compensated for, whereas in the quasi-isothermal models only longitudinal (z-direction) losses are compensated for. These assumptions lead to different internal energy profiles and different Euler equations from which the Lorentz profile of the jet is derived. In each case, we briefly explain the assumptions and list the Euler equation for the model. For a more thorough explanation, we suggest the reader refers to Crumley et al. (2017).

A1 Adiabatic jet model

In the adiabatic jet model, the jet conserves energy such that it obeys the relativistic Bernoulli equation: $\gamma_j(\omega/n) = \text{const}$. This means that $T_j \propto n^{\Gamma_{adi}-1}$. The internal energy density profile is

$$U_j(z) = \zeta n_0 m_p c^2 \left(\frac{\gamma_j \beta_j}{\gamma_0 \beta_0}\right)^{-\Gamma_{adi}} \left(\frac{z}{z_0}\right)^{-2\Gamma_{adi}}. \quad \text{(A1)}$$

The Euler equation is

$$\left(\gamma_j \beta_j \frac{\Gamma_{adi}+\xi}{\Gamma_{adi}-1} - \Gamma_{adi}\gamma_j\beta_j - \frac{\Gamma_{adi}}{\gamma_j\beta_j}\right)\frac{\partial \gamma_j \beta_j}{\partial z} = \frac{2}{z}, \quad \text{(A2)}$$

$$\xi = \frac{1}{\zeta}\left(\gamma_j\beta_j\sqrt{\frac{1+2\zeta\Gamma_{adi}-\zeta\Gamma_{adi}^2}{\zeta\Gamma_{adi}(\Gamma_{adi}-1)}}\right)^{\Gamma_{adi}-1}\left(\frac{z}{z_0}\right)^{2(\Gamma_{adi}-1)}. \quad \text{(A3)}$$

In terms of CR acceleration, adiabatic jets generally attain lower CR energies compared to other jet models, especially at large z. This is because the internal energy density and thus magnetic field strength decreases rapidly as z increases, as no re-acceleration occurs. This is seen in Fig. A1, we stress that the adiabatic jet model cannot fit the flat spectra we see in XRB jets, and is presented primarily for comparison.

A2 Isothermal jet model

In the isothermal jet model, all adiabatic losses are recompensated for and thus T_j is constant. This means that $U_p \propto n$, and energy is not conserved. The maximum energy CR energy as a function of jet height can be seen in Fig. A2.

$$U_j(z) = \zeta n_0 m_p c^2 \left(\frac{\gamma_j \beta_j}{\gamma_0 \beta_0}\right)^{-\Gamma_{adi}} \left(\frac{z}{z_0}\right)^{-2}. \quad \text{(A4)}$$

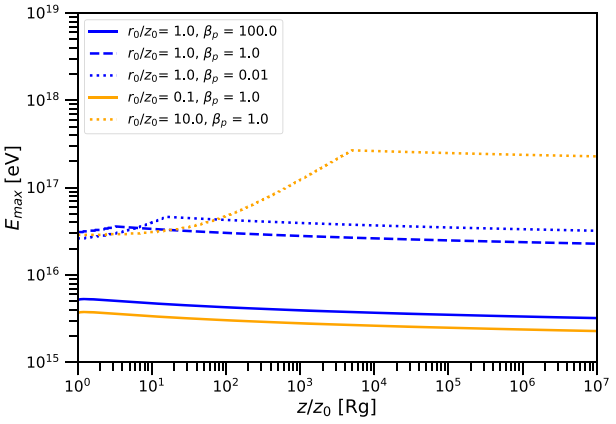

Figure A2. Maximum CR energy as a function of jet height z for the isothermal jet model.

The Euler equation is

$$\left(\gamma_j\beta_j\frac{\Gamma_{adi}+1}{\Gamma_{adi}-1}-\Gamma_{adi}\gamma_j\beta_j-\frac{\Gamma_{adi}}{\gamma_j\beta_j}\right)\frac{\partial\gamma_j\beta_j}{\partial z}=\frac{2}{z}. \tag{A5}$$

A3 Quasi-isothermal (*agnjet*) model

In the quasi-isothermal model, the gas in the jet can only do work in the z-direction, meaning that $T_j \propto (\gamma_j\beta_j)^{1-\Gamma_{adi}}$. A key difference here is that we include self-collimation, and so the radius of the jet as a function of jet height z is given by equation (11). The internal energy density profile is similar to the isothermal case:

$$U_j(z)=\zeta n_0 m_p c^2\left(\frac{\gamma_j\beta_j}{\gamma_0\beta_0}\right)^{-\Gamma_{adi}}\left(\frac{r_{coll}}{r_0}\right)^{-2}. \tag{A6}$$

Here, we use the collimated radius from equation (11). The Euler equation, however, includes an additional factor:

$$\left(\gamma_j\beta_j\frac{\Gamma_{adi}+\xi}{\Gamma_{adi}-1}-\Gamma_{adi}\gamma_j\beta_j-\frac{\Gamma_{adi}}{\gamma_j\beta_j}\right)\frac{\partial\gamma_j\beta_j}{\partial z}=\frac{2}{z}, \tag{A7}$$

$$\xi=\frac{1}{\zeta}\left(\frac{\gamma_j\beta_j}{\gamma_0\beta_0}\right)^{\Gamma_{adi}-1}. \tag{A8}$$

The figure for this jet model is found in Section 4, Fig. 4. We note that $U_j(z)$ is very similar for the isothermal and quasi-isothermal models, as only the dependence on the radius is different. For this reason, their maximum CR energies are very similar.

This paper has been typeset from a TEX/LATEX file prepared by the author.